Photoacoustics 22 (2021) 100268

Contents lists available at ScienceDirect

Photoacoustics

journal homepage: www.elsevier.com/locate/pacs

Microvascular imaging and monitoring of hemodynamic changes in the skin during arterial-venous occlusion using multispectral raster-scanning optoacoustic mesoscopy

Amalina Binte Ebrahim Attia [a,1,2], Mohesh Moothanchery [a,1,2], Xiuting Li [a,2], Yik Weng Yew [b], Steven Tien Guan Thng [b], U.S. Dinish [a,2,*], Malini Olivo [a,2,*]

[a] Laboratory of Bio Optical Imaging, Singapore Bioimaging Consortium, Agency of Science, Technology and Research (A*STAR), Singapore
[b] National Skin Centre, Singapore

ARTICLE INFO

Keywords:
Optoacoustic imaging
Occlusion
Microvasculature
Hemodynamics
Vascular diseases
Inflammatory skin diseases

ABSTRACT

The ability to monitor oxygen delivery in microvasculature plays a vital role in measuring the viability of skin tissue and the probability of recovery. Using currently available clinical imaging tools, it is difficult to observe non-invasive hemodynamic regulation in the peripheral vessels. Here we propose the use of a novel multispectral raster-scanning optoacoustic mesoscopy (RSOM) system for noninvasive clinical monitoring of hemodynamic changes in the skin microvasculature's oxy- (HbO_2) and deoxy-hemoglobin (Hb), total hemoglobin (HbT) and oxygen saturation (rsO_2). High resolution images of hemoglobin distribution in the skin microvasculature from six healthy volunteers during venous and arterial occlusion, simulating systemic vascular diseases are presented. During venous occlusion, Hb and HbO_2 optoacoustic signals showed an increasing trend with time, followed by a drop in the values after cuff deflation. During arterial occlusion, an increase in Hb value and decrease in HbO_2 values was observed, followed by a drop in Hb and jump in HbO_2 values after the cuff deflation. A decrease in rsO_2 values during both venous and arterial occlusion was observed with an increase in value after occlusion release. Using this proof of concept study, hereby we propose multispectral RSOM as a novel tool to measure high resolution hemodynamic changes in microvasculature for investigating systemic vascular diseases on peripheral tissues and also for monitoring inflammatory skin diseases, and its therapeutic interventions.

1. Introduction

Skin microcirculation consists of vessels with diameters < 150 μm, including arterioles, capillaries and venules within the superficial plexus at 400–500 μm depth and deep plexus at 1.9 mm below the skin surface [1,2]. Measuring skin microcirculation and oxidative metabolism is of interest in clinical settings as it provides information to understand multiple skin conditions, not limited to angiogenesis, neovascularization, inflammation, infection, etc [3,4] and systemic co-morbidities such as vascular diseases (e.g. cardiovascular disease) and metabolic syndromes (e.g. diabetes) [5]. Emerging evidence have shown that the cutaneous microcirculation can serve as a representative vascular bed to assess local function by examining the arterioles and venules within a defined region [6]. Systemic vascular dysfunction can be manifested in cutaneous microcirculation [7,8], reflecting the systemic dysfunction in the same extent and mechanism [9], making cutaneous microvasculature a useful surrogate model for studying vascular function and hemodynamic response. Therefore, having a non-invasive skin-specific technique to assess the local vascular function and response is desirable and potentially useful in the assessment and prognosis of dermatologic conditions and systemic vascular comorbidities.

Pulse oximetry is a widespread clinical monitoring tool that provides the measurement of oxygenated hemoglobin percentage in arterial blood by obtaining a ratio of signal in the pulsatile component of arterial blood in relation to that from tissue, venous blood, and non-pulsatile arterial blood. However, the accuracy of this technique decreases at saturation measurements below 70 %, and in hypoxic states experienced

* Corresponding authors.
E-mail addresses: dinish@sbic.a-star.edu.sg (U.S. Dinish), Malini_olivo@sbic.a-star.edu.sg (M. Olivo).
[1] Authors contributed equally.
[2] Current address: Translational Biophotonics Lab, Institute of Bioengineering and Bioimaging, Agency of Science, Technology and Research (A*STAR), Singapore

https://doi.org/10.1016/j.pacs.2021.100268
Received 28 January 2021; Received in revised form 15 April 2021; Accepted 16 April 2021
Available online 20 April 2021

in vascular diseases such as hypotension, hypothermia and reduced perfusion states due to low-amplitude pulses [10]. This is disadvantageous as the low signal-to-noise ratio in such patients will prevent accurate readings to be obtained where they are needed most. Doppler ultrasound is another widely used tool in clinics to assess blood flow [11] albeit the low contrast to the flow in smaller vessels, makes it suboptimal to measure hemodynamic changes. Magnetic resonance imaging (MRI) and positron emission tomography (PET) are promising techniques with its own advantages [12], but the poor mobility and the high cost make them non-recommended solutions. Several other clinical non-invasive imaging and sensing techniques techniques to assess the skin microcirculation includes capillaroscopy [13], videocapillaroscopy [14], thermography [15], laser Doppler flowmetry [16,17], strain gauge plethysmography (SGP) [18], transcutaneous oximetry ($tcpO_2$) [19] and near-infrared spectroscopy (NIRS) [20]. Both capillaroscopy and videocapillaroscopy are limited in penetration depth and can only access up to 200 μm below skin surface. Optical coherence tomography (OCT) adapted to skin microvasculature imaging is similarly limited in its penetration depth (~450 μm) [21]. Thermography on the other hand can only give an indirect measurement of microcirculations by relating blood flow with the recorded infrared images. SGP is a relatively simpler technique which has been used for many years for point perfusion measurements and thus unable to provide spatial images. As for $tcpO_2$, it employs the principle of inducing local hyperemia by heating while requiring repeated calibrations and a time-consuming process to set appropriate measurement conditions. Both laser Doppler flowmetry and NIRS have been used to study vascular diseases with relatively low spatial resolutions. NIRS in particular does not measure blood flow directly, complicating the interpretation of tissue oxygenation.

Optoacoustic (photoacoustic) imaging (OAI) on the other hand is a hybrid imaging modality based on the principle of thermoelastic expansion of tissue using pulsed laser excitation and ultrasound signal detection [22]. OAI has shown great potential in scalable deep tissue imaging with high spatio-temporal resolution while providing complementary functional, molecular and structural information of tissue [23]. Due to its distinct optical absorption contrast, it is increasingly playing a pivotal role in clinical and biological research with the ability to resolve main endogenous tissue absorbers i.e. hemoglobin, melanin and water. Optoacoustic signal from hemoglobin can provide vascular structural information and in vivo hemodynamic changes by utilizing the absorption contrast between oxygenated-hemoglobin (HbO_2) and deoxygenated-hemoglobin (Hb) [24]. In one such configuration of OAI systems, optoacoustic tomography has been exploited to demonstrate hemodynamic changes in muscle tissue [25,26] and foot [27] with resolutions $\geq$ 150 μm. This configuration however is not enough to resolve skin microvasculature in high resolution. Another configuration of OAI system, optoacoustic microscopy could enable microvascular imaging and demonstrated vascular response during arterial occlusion by using two wavelengths [28] while another study reported using a single wavelength on the vascular hemodynamic during venous occlusion [29]. However, the reported optoacoustic microscopy did not manage to resolve the changes in Hb and HbO_2 in individual vessels and its relation to venous and arterial occlusion.

Raster-scanning optoacoustic mesoscopy (RSOM) is a novel OAI system configuration that offers ultrawideband ultrasound detection to yield high resolution (10 and 40 μm, axial and lateral resolutions respectively) images up to a few millimeters deep with a single wavelength excitation. It has been successfully employed to clinically image [30] cutaneous inflammatory skin diseases such as psoriasis [31] and atopic dermatitis [32] and nailfold microvasculature [33]. When fitted with a tunable laser, the RSOM system is capable of resolving the tissue absorbers, giving a spatial map and relative concentration of the absorbers [34]. By quantifying the levels of Hb and HbO_2 signals, the oxygenation status (rsO_2) of the bulk vascular structure and individual vessels can be determined. This multispectral RSOM setup yielded mean oxygen saturation values of 85 $\pm$ 4 % in superficial vessels and about 54 $\pm$ 7 % in a deeper vessel in the dermis of the forearm, similar to the bulk oxygen saturation values obtained from other optical measurements such as reflectance spectroscopy and NIRS in the same area [34]. Evidently, multispectral RSOM has demonstrated its potential in imaging microvasculature and its oxygenation status at different depths and at specific locations of the skin layers, unlike pulse oximetery. The quantification of the vascular features is also possible down to individual vessels in the 3D images while pulse oximetry gives a bulk saturation value. Because optoacoustic imaging is not dependent on pulsatile of blood vessels and rather on the absorbance of chromophores, their quantification of hypoxic states is still possible from the spatial Hb and HbO_2 signals. The aim of this study is to demonstrate the capability of high-resolution multispectral RSOM technique for monitoring hemodynamic changes in the microvasculature of the forearm during cuff occlusion, simulating ischemic and thrombosis conditions.

2. Methods

2.1. Subjects and protocols

Healthy adult volunteers (n = 6) of Fitzpatrick skin types II to IV participated in this study which was approved by National Healthcare Group Domain Specific Review Board 2020/00079, Singapore. In this study, the subjects were in a sitting position on a chair with their arm outstretched and resting at heart level. The imaging head was placed by a flexible mechanical arm over the right forearm at mid-point between hand and elbow on the volar forearm. A blood pressure cuff was attached around the right upper arm. The forearm was upward and supported by a pillow. The cuff occlusion protocol for the subjects are detailed in Fig. 1. Briefly, the venous-arterial occlusion challenges comprised of seven stages. First, a baseline image was captured from the volunteer in the resting state before occlusion (i). Second, venous outflow was stopped using an occlusion cuff, by inflating the cuff up to 80 mm Hg pressures and an image was captured at 1 min venous occlusion (ii). Third, another image was captured at 3 min venous occlusion ((iii)). Fourth, the occlusion cuff was deflated rapidly and an image was captured at 2 min post-release (iv). Fifth, both venous outflow and arterial inflow was stopped by inflating the cuff and an image was captured at 1 min arterial occlusion (v). The arterial occlusion pressure used was 40 mm Hg more than that of systolic pressure. Sixth, another image was captured at 3 min arterial occlusion (vi). Finally, the occlusion cuff was deflated rapidly and an image was captured at 2 min post-release (vii). To minimize movements of the imaging area, the arm was rested on a flat surface while the volunteers sat on a chair without wheels comfortably.

2.2. Multispectral optoacoustic mesoscopic imaging system

An RSOM Explorer ms-C50 system (iThera Medical GmbH, Munich, Germany) was used for optoacoustic imaging. Briefly, the skin was illuminated with a multispectral, nanosecond pulsed, Raman laser having four different wavelengths (532, 555, 579, 606 nm) and 2.5-3.2 ns pulse width. The time difference between successive pulses is in the range of 0.5–2 ms. The repetition rate of the laser can be varied between 325 Hz per wavelength to a maximum of 1.3 kHz for all wavelengths, depending on the field of view and number of wavelengths used. The laser light with a pulse energy ~25 μJ was delivered through a single customized fiber for optimum light illumination which combined with a broadband spherically focused transducer (50 MHz center frequency, 11−99 MHz bandwidth, 4 mm focal diameter, 4 mm active element distance, f-number: 1). The combined illumination detector system was attached to a two axis motorized stage enabling raster scanning the two-dimensional (2D) field of view of up to 6 × 6 mm with a step size of 20 μm, which forms the scanning head. The scanning head was attached at the end of an articulated arm for optimal positioning. A water-filled unit with the bottom covered with an interchangeable polyethylene

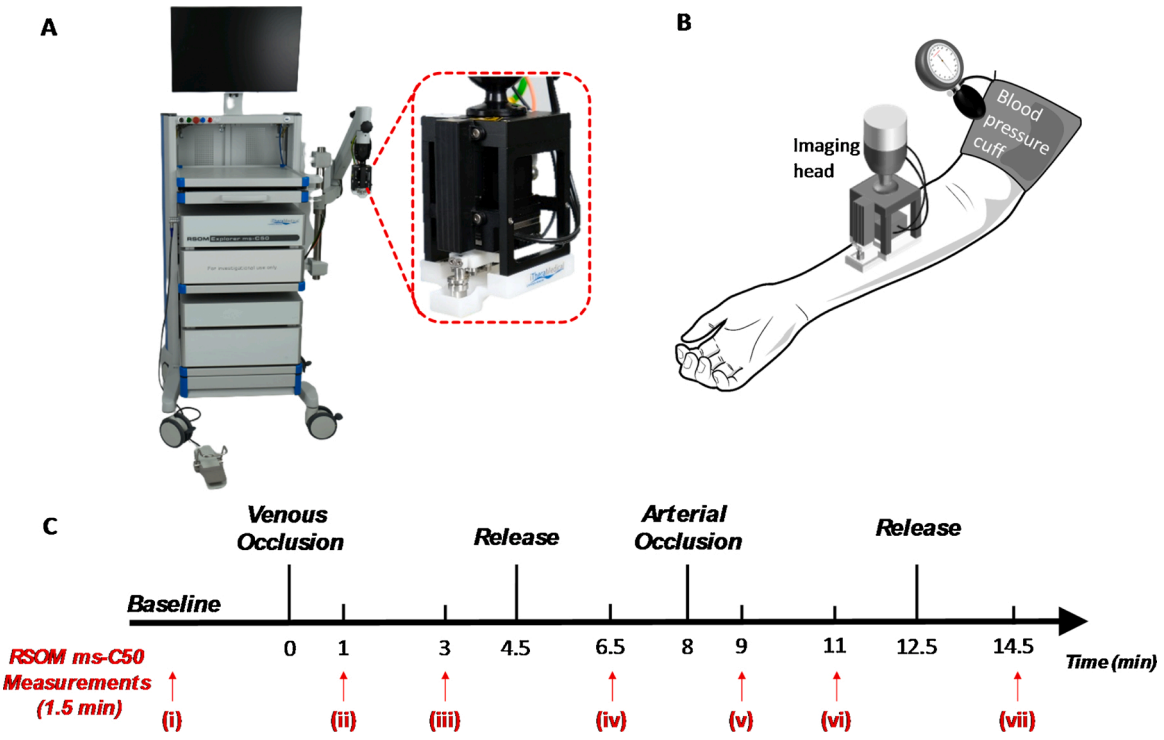

Fig. 1. Experimental system, protocol and timeline for the venous and arterial occlusion challenges. (A) Photograph of the RSOM ms-C50 clinical prototype system with insert showing the scanning head; (B) Schematic showing the imaging head position and location of blood pressure cuff on subjects' arms; (C) Experimental timeline of venous and arterial occlusion challenges showing the various time points (i - vii) at which RSOM ms-C50 images were acquired.

membrane will connect the scan head to the skin surface by means of ultrasound gel. All the imaging parameters were within maximum permissible exposure (MPE) limits and the system was equipped with a key switch, a laser safety foot pedal and an emergency off button for safe operation of the laser. The data acquired were amplified using two low noise amplifiers of 30 dB (one pre and one post data detection).

2.3. Image processing

The recorded optoacoustic signals were subsequently reconstructed with a beam-forming algorithm by assuming the fact that at the focal point of the transducer, a point detector is located, which accepts signals within a cone with its angle defined by the numerical aperture of the transducer. To facilitate the visualization of the skin layers and vascular structures, the skin surface was identified and then flattened with motion correction to reduce the motion effects from the subjects [35,36]. The flattened and motion corrected reconstructed images were unmixed by linear regression for different absorbers namely melanin, Hb, and HbO_2 using all four available wavelengths. Two frequency sub-bands are divided from optoacoustic signals for concurrent visualization of bigger and smaller vascular structures, in which low frequency band (LF) was colored in red from 11 to 33 MHz representing bigger structures, high frequency band (HF) was colored in green from 33 to 99 MHz representing smaller structures. The 3D volume images and maximum intensity projection (MIP) images along the depth direction (z-axis) were generated for further processing. By averaging all the pixels in the x-y plane along the depth, the multispectral RSOM optoacoustic profile along the skin depth was obtained. The depth ranges of epidermis (E) and dermis (D) regions was segmented manually based on the optoacoustic MIP profiles along the depth direction.

2.4. Data analysis

The quantification of each absorber's optoacoustic signal was calculated by averaging all the voxels in the 3D volume of multispectral RSOM images. The total hemoglobin (HbT) and oxygen saturation (rsO_2) were then calculated by the equations Hb + HbO_2 and HbO_2/ (Hb + HbO_2) respectively. The plots of absorber values for all the subjects at various time points over the period of occlusion challenges were presented. Data were presented as mean ± standard error of the mean (SEM) values. Two-sided paired t-test was used to compare variables with $p < 0.05$ regarded as statistically significant. The calculation was also applied on a small demarcated area with individual vessels of one subject to validate the sensitivity of multispectral RSOM, and on LF and HF bands of the same subject to explore the bigger and smaller vascular structures changes during the occlusion challenges.

3. Results and discussion

3.1. Multispectral optoacoustic images of the forearm during occlusion challenge

Fig. 1 shows the cuff occlusion challenge protocol and the various discrete time points at which multispectral RSOM imaging of the forearm was acquired during the occlusion challenge, labelled as (i) to (vii). The corresponding and representative multispectral RSOM MIP images are shown in Fig. 2 with each hemoglobin absorber shown separately and merged together with melanin absorber in the xz plane. The blood oxygen saturation (rsO_2) maps of the MIPs at each time point are also shown in Fig. 2. The multispectral RSOM was capable of resolving the structural architecture of the skin with the images showing melanin in uppermost epidermis (green) layer with a present hair shaft followed by the dermis layer underneath. The epidermal layer is characterized mainly by strong absorption of melanin signals with minimal presence of hemoglobin absorption. On the other hand, the contribution from melanin in the dermis was not present, as expected. The vascular plexus network could be visualized in the dermis showing the spatial maps of optoacoustic signals of HbO_2 and Hb, from which the rsO_2 map could be derived. At baseline (i), the rsO_2 values for the representative case in Fig. 2 were in the range between 65 % and 92 % over the skin depth.

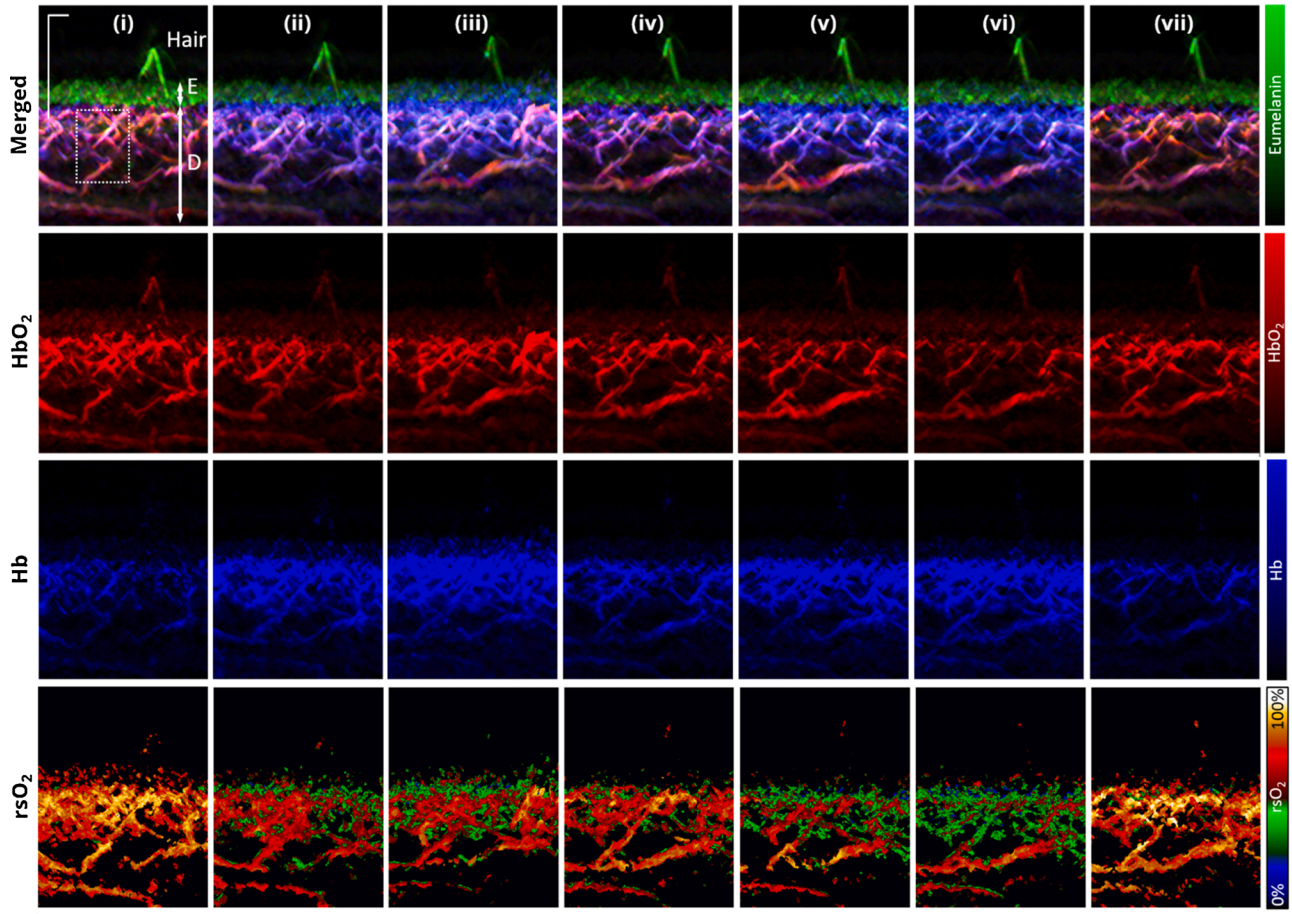

Fig. 2. Multispectral optoacoustic mesoscopic imaging of forearm during venous and arterial occlusion challenges. Maximum intensity projection (MIP) RSOM ms-C50 images at time points (i) to (vii) showing the merged HbO_2 (red), Hb (blue) and eumelanin (green) spatial map and individual HbO_2 (red), Hb (blue) and rsO_2 maps. The layers demarcating the epidermis, E and dermis, D is indicated with white arrows. Scale bar; 500 μm.

In general, the Hb optoacoustic signals increased in intensity (blue signals) during occlusion of venous or arterial flow and dropped close to baseline values 2 min post-release of occlusion (Fig. 2). The time point at which the Hb optoacoustic signals were the highest was at (iii) at which 3 min venous occlusion occurred compared to the arterial occlusion challenge. On the other hand, the HbO_2 optoacoustic signals peaked at time point (iii) with vessel dilation present for some individual vessels and was the lowest at time point (iv) (Fig. 2). In the rsO_2 spatial maps, the rsO_2 change during the venous and arterial occlusion challenges was only observed in the dermis as vascular supply is not present in the epidermis. The baseline (i) rsO_2 values in the dermis were above 50 % in the heat map while an increase of signals signifying less than 50 % rsO_2 was observed during both occlusions in the spatial maps. Notably, the 3 min arterial occlusion time point (vi) exhibited the highest number of signals signifying less than 50 % rsO_2.

Depth-dependent oxygen saturation can be observed from the spatial heat maps of rsO_2 values in Fig. 2. At time points (i) and (vii) i.e. the baseline and recovery from occlusion challenge respectively, the highest rsO_2 values were seen in the vessels of superficial plexus just underneath the epidermis. During arterial occlusion (time points (v) and (vi)), the highest rsO_2 values were observed in the deeper vessels instead. Atmospheric oxygen being taken up by the skin through diffusion is well-documented, reaching a depth of 0.25 to 0.40 mm from the skin surface [37] explaining why the superficial plexus vessels exhibited the higher oxygen saturation values at baseline and post-occlusion.

3.2. *Venous occlusion challenge*

Fig. 3 shows the mean optoacoustic signals of Hb, HbO_2, HbT and calculated rsO_2 values over the occlusion challenges for the subjects ($n = 6$). During the venous occlusion challenge (time points (i) to (iv)) whereby the venous outflow is impeded while the arterial supply is retained, an increase in Hb, HbO_2 and HbT optoacoustic signals was observed (Fig. 3A-C). The maximum Hb, HbO_2 and HbT optoacoustic signals occurred at time point (iii), i.e. the 3rd minute of venous occlusion (increase by 403 %, 41 % and 112 % respectively compared to baseline (i)). The increase in HbT was probably due to the increase in blood volume when the blood accumulates from the blocked venous outflow during the occlusion. Notably, the increase in Hb signals is more drastic than that of HbO_2 signals. At timepoint (iv) i.e. 2 min post cuff release, the Hb, HbO_2 and HbT optoacoustic signals decreased from their peak values at time point (iii) to 38.9 %, -17.9 % and -5.9 % of baseline (i) values respectively, indicating venous drainage had resumed.

The mean oxygen saturation level decreased from 74.2 % at baseline to 58.9 % at 1 min post occlusion before further decreasing to 50.2 % at 3 min post-occlusion (Fig. 3D). While both Hb and HbO_2 signals increased during venous occlusion due to the accumulation of blood, the drastic increase in Hb signals compared to that of HbO_2 signals resulted in a decrease in oxygen saturation levels during the occlusion period. This can be attributed to the disruption of transport of deoxygenated blood from the peripheral blood vessels back to the lungs for the exchange of carbon dioxide for oxygen while blood is accumulating during the occlusion. The increase in HbO_2 signals was slower probably due to the increasing intraluminal blood pressure with the increased volume of

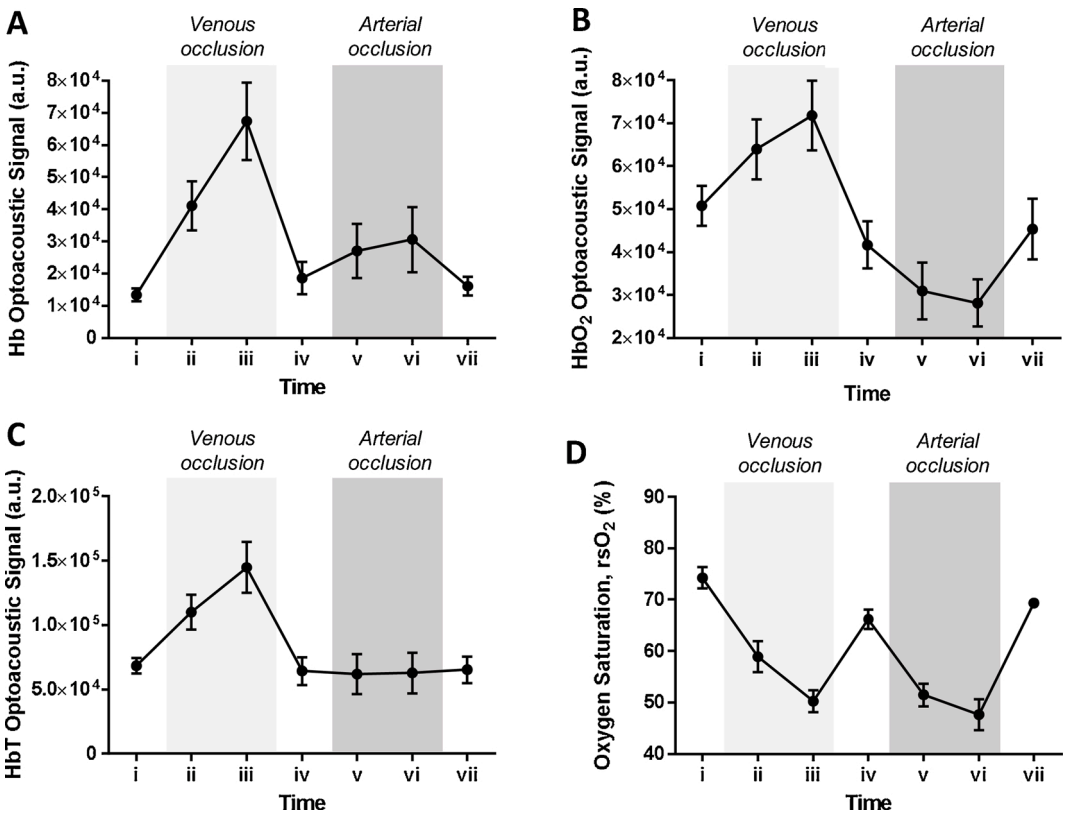

Fig. 3. Quantitative analysis of multispectral optoacoustic mesoscopic images of forearm during venous and arterial occlusion challenges. Plots of (A) Hb, (B) HbO_2, (C) HbT optoacoustic signals and (D) rsO_2 values for the subjects ($n = 6$) over the occlusion challenges period (mean ± SEM). Time points (i) to (iv) corresponds to venous occlusion challenge with time point (iv) representing release of the occlusion. Time points (iv) to (vii) correspond to arterial occlusion challenge with time point (vii) representing release of the occlusion.

blood which can gradually reduce the arterial inflow. At 2 min post cuff release (iv), the oxygen saturation level rebounded to a mean value of 66.2 % while still not recovering near to the baseline values ($p = 0.024$ compared to baseline values). This can be attributed to the fact that HbO_2 signals only recovered to below baseline values upon cuff release. As venous drainage resumes after cuff release, the blood volume will decrease, leading to the decrease of Hb and HbO_2 signals. However, the strong drainage of the accumulated blood was probably propelled by the intraluminal blood pressure achieved during the venous occlusion challenge, thereby reducing the HbO_2 signals before ultimately achieving baseline values.

3.3. Arterial occlusion challenge

During the arterial occlusion challenge (time points (iv) to (vii)) whereby both the venous outflow and arterial inflow are interrupted, an increase in Hb and a decrease in HbO_2 optoacoustic signals were observed (Fig. 3A-B). At the 3rd min of the occlusion challenge i.e. time point (vi), Hb signals increased to 64.4 % of that of time point (iv) while HbO_2 signals decreased by 32.5 % of that of time point (iv). HbT optoacoustic signals on the other hand remained steady (within 2.5 % of that of time point (iv)) throughout the occlusion challenge period as no change in blood volume was expected with no outflow and inflow of blood occurring (Fig. 3C). The simultaneous increase in Hb and decrease in HbO_2 signals during arterial occlusion is indicative of the blood oxygen consumption in the blood vessels with no supply of oxygenated blood being delivered i.e. towards tissue hypoxia. Upon release of the cuff, both Hb and HbO_2 signals returned within 10 % of that of time point (iv). While it is expected to observe a rebound hyperemia effect in response to pro-vasodilatory molecules secreted to increase blood flow to meet the oxygen demand, this was not observed in this study. The RSOM ms-C50 system is limited to time-point measurements due to the raster-scanning of the imaging site during image acquisition and the hyperemia effect may have been only apparent immediately post-cuff release which was not captured during image acquisition.

Similar to the venous occlusion challenge, the mean oxygen saturation level decreased during the arterial occlusion challenge, from 66.2 % at time point (iv) to a minimum of 47.6 % at 3 min of arterial occlusion (time point (vi)) before recovering to 69.4 % at 2 min post cuff release (Fig. 3D). The decrease in oxygen saturation level is due to the cutaneous oxygen consumption in maintaining metabolism in the vessels with limited delivery of oxygenated blood. Notably, the mean oxygen saturation values during arterial occlusion is lower than that of venous occlusion probably due to the interrupted inflow of oxygenated blood in the former.

3.4. Sensitivity of multispectral RSOM imaging

While Fig. 3 was obtained from bulk calculations of Hb and HbO_2 signals from the acquired multispectral RSOM images, we also investigated the sensitivity of the system on measuring the hemodynamic variations in single vessels in a small area. The Hb, HbO_2 and HbT signals in a small area of the vascular plexus as demarcated in Fig. 2 in a white dashed box were calculated for all the time points in one representative subject (Fig. 4). Fig. 4A shows that in a small area of interrogation for one subject, the trends of Hb, HbO_2 and HbT hemodynamic changes were consistent with that of Fig. 3, which was calculated from the bulk vasculature in the images and averaged among all the subjects. The Hb, HbO_2 and HbT signals peaked at time point (iii) during the 3rd min of venous occlusion in Fig. 4A. The Hb signals increased during arterial occlusion whereas the HbO_2 signals decreased during the challenge instead compared to that of time point (iv). Similarly, the rsO_2

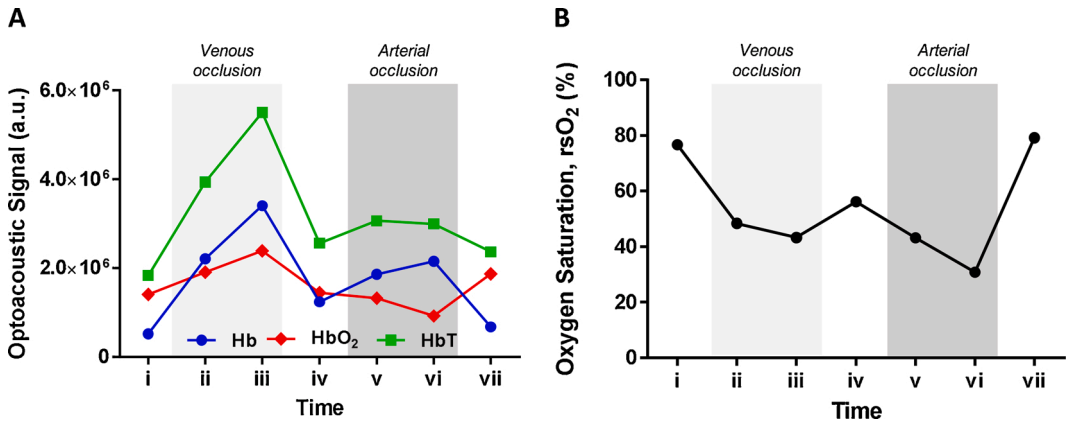

Fig. 4. Validating sensitivity of multispectral RSOM. Dotted white box in Fig. 2 showing the area with individual vessels for tracking the (A) Hb, HbO2 and HbT signals and (B) rsO_2 values in one small area in one representative subject over the time points. Time points (i) to (iv) corresponds to venous occlusion challenge with time point iv representing release of the occlusion. Time points (iv) to (vii) corresponds to arterial occlusion challenge with time point vii representing release of the occlusion.

values of the vessels in the small area followed the same hemodynamic variation with that of the bulk vasculature. The rsO_2 values decreased from the baseline value during both occlusion challenges with the lowest being at time point (vi) i.e. 3rd min of arterial occlusion. Recovery of oxygen saturation after venous occlusion did not reach baseline values while recovery after arterial occlusion did, similar to that observed in the bulk quantification of oxygen saturation. Thus, the multispectral RSOM technique demonstrates promise and sensitivity for visualizing and quantifying the hemodynamic responses in single vessels in a small area of interrogation.

In Fig. 3D, a decrease of 26 % in the rsO_2 was observed between baseline and its minimum value at time point (vi). In comparison, a decrease of 45 % in the rsO_2 values was observed between baseline and that of time point (vi) in Fig. 4B. While the hemodynamic trends of the vessels in the small area were comparable to that of bulk vasculature, this difference in rsO_2 reductions between the vessels in the small area and bulk vasculature is significant. Firstly, this is probably due to the difference in the relative vasculature signal in relation to the background signals in the region-of-interest in both the small area and bulk volume. The defined small area was vasculature rich i.e. the density of the Hb and HbO_2 signals were higher compared to the non-vascular background. This will enhance the contrast between the vasculature and background hemoglobin signals. Thus, the reduction of rsO_2 during the occlusion challenge was more pronounced in the small area than that of the bulk volume. One way to address this limitation is by segmenting the vessels from the background in rsO_2 calculations. This requires a higher frequency transducer to effectively increase the resolution of the outline of the vascular structures for easier segmentation. Secondly, the selected small area in which the rsO_2 were quantified was near the skin surface compared to the overall bulk vasculature measurements in the

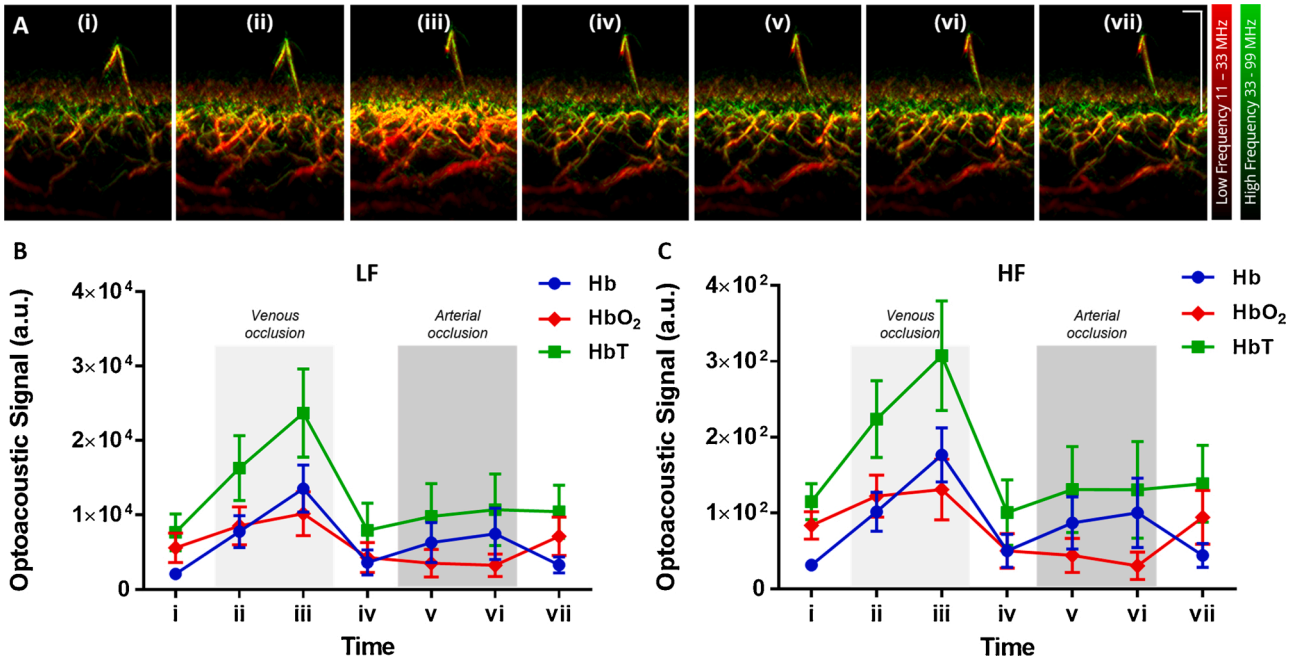

Fig. 5. The ultrawide detection bandwidth of multispectral RSOM divided into low (LF) and high frequency (HF) bands. (A) Representative cross-sectional multispectral RSOM images at various time points (i to vii) of venous and arterial occlusion challenges with concurrent visualization of LF band (11 – 33 MHz) in red and HF band (33–99 MHz) in green at single wavelength 532 nm. Bigger vascular structures are shown in LF band while smaller vascular structures in HF band. Plots of unmixed Hb, HbO_2 and HbT optoacoustic signals for (B) LF and (C) HF bands for the subjects ($n = 6$) over the occlusion challenges period (mean ± SEM). Scale bar; 500 μm.

3D volume. As the incident light reaching the dermis gets lower with the increasing depth, the changes in rsO_2 values of the deeper dermis vessels captured from optical imaging would be less sensitive. Therefore, the rsO_2 values in the selected small area will vary significantly during occlusion compared to the averaged values in the overall 3D bulk volume. Vogt et al. have similarly reported that the accuracy of oxygen saturation measurement is depth-dependent, which is attributed to fluence artifacts [38].

3.5. Low and high-frequency bands of multispectral RSOM images

With a broadband transducer fitted in the multispectral RSOM system, the detected ultrasound signals can be divided into two separate frequency bands for better visualization. The cross-sectional multispectral RSOM images for the same representative subject is shown in Fig. 5A in which the low (LF) and high frequency (HF) components acquired at single wavelength 532 nm are labelled in red and green respectively. The plots of the LF and HF components of the unmixed Hb, HbO_2 and HbT signals are shown in Fig. 5B-C. Larger vascular structures are shown in LF band (~20 to 50 μm in size for 11−33 MHz) while smaller vascular structures are visualized in HF band (~10 to 20 μm in size for 33−99 MHz). Any overlap of both frequency bands will result in yellow signals. The multispectral RSOM images in Fig. 5A revealed a depth-dependent variation of blood vessel size. In the cross-sectional images, the HF band signals are present in the vessels immediately underneath the epidermis. In the depth axis direction, the frequency band signals turn to yellow indicating a presence of LF band signals followed by predominantly red LF band signals deeper to the hypodermis. This was especially apparent in time point (iii) of Fig. 5A. It is known that arterioles deeper in the dermis are larger in diameter than that near the dermal papillae.

During venous occlusion, the LF and HF signals at 532 nm (Fg. 5A) and of HbT absorber (Fig. 5B-C) increased in intensity compared to that of baseline with the signals most intense at time point (iii) (209 % and 167 % change from baseline, respectively for HbT). The signals decreased upon release of occlusion at time point (iv). However, during arterial occlusion, no discernible differences in the LF and HF signals at 532 nm were observed among time points (iv) to (vii) (Fig. 5A). While it was shown previously that accumulation of blood occurs during venous occlusion, it demonstrates herein that both small and big vessels exhibited the same hemodynamic response to the venous occlusion challenge. The increase in both LF and HF signals signify vessel dilation occurring upon obstruction of venous outflow. As both outflow and inflow of blood was impeded in arterial occlusion, no change in LF and HF signals were expected. Similarly, when the individual absorber signals were divided into LF and HF bands in Fig. 5B-C, both frequency bands show similar trend of hemodynamic response for Hb, HbO_2 and HbT absorbers.

4. Conclusion

In this study, we present a novel high-resolution multispectral optoacoustic system and its application to image skin microvasculature and monitor hemodynamic changes. The system performance has been validated under physiological interventions such as venous and arterial cuff occlusion challenges to simulate systemic vascular conditions in the skin from six healthy volunteers. During both venous and arterial occlusion, Hb optoacoustic values showed an increasing trend with time compared to baseline, whereas HbO_2 values showed an increasing trend during venous occlusion, and decreasing trend during arterial occlusion, compared to baseline. The rsO_2 values decreased during both venous and arterial occlusions. The optoacoustic absorber signals and rsO_2 values recovered near to baseline values upon release of occlusion. An accumulation of blood was observed during venous occlusion in both smaller and bigger vessels in the vascular plexus leading to their dilation during the occlusion challenge. The hemodynamic trends were also observed in single vessels in a small defined region of monitoring, corroborating multispectral RSOM's sensitivity to detect absorber signals in single vessels. Thus, multispectral RSOM has demonstrated its potential as a novel clinical imaging tool to measure hemodynamic changes in peripheral tissue microvasculature. Understanding the hemodynamic response in the vessels of peripheral tissues using imaging techniques present a novel way of non-invasive investigation of systemic vascular diseases. Additionally, the ability to monitor microcirculation and changes in blood oxygenation at different depths below the skin surface at high resolution opens the window of opportunity for non-invasive evaluation of various inflammatory skin diseases and conditions in which vascular remodeling is commonly observed [39]. In this context, we envision that this study will open up new avenues in understanding inflammatory skin conditions such as eczema and psoriasis and its associated comorbidities

Funding

This work was supported by the National Medical Research Council [grant number OFIRG18nov-0101]; Agency of Science, Technology and Research (A*STAR), under its Industry alignment fund pre-positioning programme, Award H19H6a0025 and the intramural funding from Biomedical Research Council (BMRC), A*STAR, Singapore.

Declaration of Competing Interest

The authors declare that they have no known competing financial interests or personal relationships that could have appeared to influence the work reported in this paper.

Acknowledgments

This work was supported by the National Medical Research Council [grant number OFIRG18nov-0101]; Agency of Science, Technology and Research (A*STAR), under its Industry alignment fund pre-positioning programme, Award H19H6a0025 and the intramural funding from Biomedical Research Council (BMRC), A*STAR, Singapore. The authors would like to thank Mr. Douglas Goh for preparing the schematic in Fig. 1. Authors would also like to acknowledge the SBIC-iThera Medical joint lab for their support.

References

[1] M.P. De Boer, R.I. Meijer, N.J. Wijnstok, A.M. Jonk, A.J. Houben, C.D. Stehouwer, Y.M. Smulders, E.C. Eringa, E.H. Serné, Microvascular dysfunction: a potential mechanism in the pathogenesis of obesity-associated insulin resistance and hypertension, Microcirculation 19 (2012) 5–18, https://doi.org/10.1111/j.1549-8719.2011.00130.x.

[2] J. Neubauer-Geryk, M. Hoffmann, M. Wielicka, K. Piec, G. Kozera, M. Brzeziński, L. Bieniaszewski, Current methods for the assessment of skin microcirculation: part 1, Postepy Dermatol. Alergol. 36 (2019) 247–254, https://doi.org/10.5114/ada.2019.83656.

[3] D. Seth, K. Cheldize, D. Brown, E.F. Freeman, Global burden of skin disease: inequities and innovations, Curr. Dermatol. Rep. 6 (2017) 204–210, https://doi.org/10.1007/s13671-017-0192-7.

[4] X. Zhang, A. Wang, T. Shi, J. Zhang, H. Xu, D. Wang, L. Feng, The psychosocial adaptation of patients with skin disease: a scoping review, BMC Public Health 19 (2019) 1404, https://doi.org/10.1186/s12889-019-7775-0.

[5] G.L. Semenza, Oxygen sensing, hypoxia-inducible factors, and disease pathophysiology, Annu. Rev. Pathol. 9 (2014) 47–71, https://doi.org/10.1146/annurev-pathol-012513-104720.

[6] L.A. Holowatz, C.S. Thompson-Torgerson, W.L. Kenney, The human cutaneous circulation as a model of generalized microvascular function, J. Appl. Physiol. 105 (2008) 370–372, https://doi.org/10.1152/japplphysiol.00858.2007.

[7] A. Alexandroff, M. Pauriah, R. Camp, C. Lang, A. Struthers, D. Armstrong, More than skin deep: atherosclerosis as a systemic manifestation of psoriasis, Br. J. Dermatol. 161 (2009) 1–7, https://doi.org/10.1111/j.1365-2133.2009.09281.x.

[8] I.H. Lindstedt, M.L. Edvinsson, L. Evinsson, Reduced responsiveness of cutaneous microcirculation in essential hypertension–a pilot study, Blood Press. 15 (2006) 275–280, https://doi.org/10.1080/08037050600996586.

[9] C.J. Abularrage, A.N. Sidawy, G. Aidinian, N. Singh, J.M. Weiswasser, S. Arora, Evaluation of the microcirculation in vascular disease, J. Vasc. Surg. 42 (2005) 574–581, https://doi.org/10.1016/j.jvs.2005.05.019.

[10] J.E. Sinex, Pulse oximetry: principles and limitations, Am. J. Emerg. Med. 17 (1999) 59–66, https://doi.org/10.1016/S0735-6757(99)90019-0.
[11] A.A. Oglat, M.Z. Matjafri, N. Suardi, M.A. Oqlat, M.A. Abdelrahman, A.A. Oqlat, A review of medical doppler ultrasonography of blood flow in general and especially in common carotid artery, J. Med. Ultrasound 26 (2018) 3–13, https://doi.org/10.4103/JMU.JMU_11_17.
[12] H.A.J. Struijker-Boudier, A.E. Rosei, P. Bruneval, P.G. Camici, F. Christ, D. Henrion, B.I. Lévy, A. Pries, J.-L. Vanoverschelde, Evaluation of the microcirculation in hypertension and cardiovascular disease, Eur. Heart J. 28 (2007) 2834–2840, https://doi.org/10.1093/eurheartj/ehm448.
[13] G.P. Fonseca, F.M. Brenner, S. Muller Cde, A.L. Wojcik, Nailfold capillaroscopy as a diagnostic and prognostic method in rosacea, An. Bras. Dermatol. 86 (2011) 87–90, https://doi.org/10.1590/s0365-05962011000100011.
[14] M. Hughes, T. Moore, N. O'Leary, A. Tracey, H. Ennis, G. Dinsdale, A. Murray, C. Roberts, A.L. Herrick, A study comparing videocapillaroscopy and dermoscopy in the assessment of nailfold capillaries in patients with systemic sclerosis-spectrum disorders, Rheumatology 54 (2015) 1435–1442, https://doi.org/10.1093/rheumatology/keu533.
[15] J. Christensen, L.H. Matzen, M. Vaeth, S. Schou, A. Wenzel, Thermography as a quantitative imaging method for assessing postoperative inflammation, Dentomaxillofac. Radiol. 41 (2012) 494–499, https://doi.org/10.1259/dmfr/98447974.
[16] H. Lenasi, Assessment of human skin microcirculation and its endothelial function using laser doppler flowmetry, in: O.F. Erondu (Ed.), Medical Imaging, IntechOpen, London, 2011, pp. 271–296.
[17] V.V. Osadchyi, T.I. Stanishevska, O.I. Gorna, R.M. Gorbatiuk, I.M. Melnychuk, N. L. Chernyaschuk, I.M. Kobylianska, O.V. Stoliarenko, Z. Omiotek, A. Shortanbayeva, Method of Using Laser Doppler Flowmetry in Assessment of the State of Blood Microcirculation System, Optical Fibers and Their Applications 2020, International Society for Optics and Photonics, 2020, p. 114560J.
[18] L.C. Pallarés, C.R. Deane, S.V. Baudouin, T.W. Evans, Strain gauge plethysmography and doppler ultrasound in the measurement of limb blood flow, Eur. J. Clin. Invest. 24 (1994) 279–286, https://doi.org/10.1111/j.1365-2362.1994.tb01086.x.
[19] M.M. Kmiec, H. Hou, M. Lakshmi Kuppusamy, T.M. Drews, A.M. Prabhat, S. V. Petryakov, E. Demidenko, P.E. Schaner, J.C. Buckey, A. Blank, P. Kuppusamy, Transcutaneous oxygen measurement in humans using a paramagnetic skin adhesive film, Magn. Reson. Med. 81 (2019) 781–794, https://doi.org/10.1002/mrm.27445.
[20] S. Jones, S.T. Chiesa, N. Chaturvedi, A.D. Hughes, Recent developments in near-infrared spectroscopy (nirs) for the assessment of local skeletal muscle microvascular function and capacity to utilise oxygen, Artery Res. 16 (2016) 25–33, https://doi.org/10.1016/j.artres.2016.09.001.
[21] Q. Wang, P. Gong, B. Cense, D.D. Sampson, Short-time series optical coherence tomography angiography and its application to cutaneous microvasculature, Biomed. Opt. Express 10 (2019) 293–307, https://doi.org/10.1364/BOE.10.000293.
[22] M. Moothanchery, R. Bi, J.Y. Kim, G. Balasundaram, C. Kim, M.C. Olivo, High-speed simultaneous multiscale photoacoustic microscopy, J. Biomed. Opt. 24 (2019) 1–7, https://doi.org/10.1117/1.JBO.24.8.086001.
[23] A.B.E. Attia, G. Balasundaram, M. Moothanchery, U. Dinish, R. Bi, V. Ntziachristos, M. Olivo, A review of clinical photoacoustic imaging: current and future trends, Photoacoustics 16 (2019) 100144, https://doi.org/10.1016/j.pacs.2019.100144.
[24] M. Li, Y. Tang, J. Yao, Photoacoustic tomography of blood oxygenation: a mini review, Photoacoustics 10 (2018) 65–73, https://doi.org/10.1016/j.pacs.2018.05.001.
[25] A. Karlas, M. Kallmayer, N.-A. Fasoula, E. Liapis, M. Bariotakis, M. Krönke, M. Anastasopoulou, J. Reber, H.-H. Eckstein, V. Ntziachristos, Multispectral optoacoustic tomography of muscle perfusion and oxygenation under arterial and venous occlusion: a human pilot study, J. Biophotonics 13 (2020), e201960169, https://doi.org/10.1002/jbio.201960169.
[26] J. Yang, G. Zhang, W. Chang, Z. Chi, Q. Shang, M. Wu, T. Pan, L. Huang, H. Jiang, Photoacoustic imaging of hemodynamic changes in forearm skeletal muscle during cuff occlusion, Biomed. Opt. Express 11 (2020) 4560–4570, https://doi.org/10.1364/BOE.392221.
[27] J. Yang, G. Zhang, Q. Shang, M. Wu, L. Huang, H. Jiang, Detecting hemodynamic changes in the foot vessels of diabetic patients by photoacoustic tomography, J. Biophotonics 13 (2020), e202000011, https://doi.org/10.1002/jbio.202000011.
[28] C.P. Favazza, L.A. Cornelius, L.V. Wang, In vivo functional photoacoustic microscopy of cutaneous microvasculature in human skin, J. Biomed. Opt. 16 (2011), https://doi.org/10.1117/1.3536522, 026004-026004.
[29] P. Subochev, A. Orlova, E. Smolina, A. Kirillov, N. Shakhova, I. Turchin, Raster-scan optoacoustic angiography reveals 3d microcirculatory changes during cuffed occlusion, Laser Phys. Lett. 15 (2018), https://doi.org/10.1088/1612-202X/aa9f68/meta.
[30] B. Hindelang, J. Aguirre, M. Schwarz, A. Berezhnoi, K. Eyerich, V. Ntziachristos, T. Biedermann, U. Darsow, Non-invasive imaging in dermatology and the unique potential of raster-scan optoacoustic mesoscopy, J. Eur. Acad. Dermatol. Venereol. 33 (2019) 1051–1061, https://doi.org/10.1111/jdv.15342.
[31] J. Aguirre, M. Schwarz, N. Garzorz, M. Omar, A. Buehler, K. Eyerich, V. Ntziachristos, Precision assessment of label-free psoriasis biomarkers with ultra-broadband optoacoustic mesoscopy, Nat. Biomed. Eng. 1 (2017) 1–8, https://doi.org/10.1038/s41551-017-0068.
[32] Y.W. Yew, U. Dinish, A.H.Y. Kuan, X. Li, K. Dev, A.B.E. Attia, R. Bi, M. Moothanchery, G. Balasundaram, J. Aguirre, V. Ntziachristos, M. Olivo, S.T. G. Thng, Raster-scanning optoacoustic mesoscopy (rsom) imaging as an objective disease severity tool in atopic dermatitis patients, J. Am. Acad. Dermatol. (2020), https://doi.org/10.1016/j.jaad.2020.06.045.
[33] J. Aguirre, B. Hindelang, A. Berezhnoi, U. Darsow, F. Lauffer, K. Eyerich, T. Biedermann, V. Ntziachristos, Assessing nailfold microvascular structure with ultra-wideband raster-scan optoacoustic mesoscopy, Photoacoustics 10 (2018) 31–37, https://doi.org/10.1016/j.pacs.2018.02.002.
[34] M. Schwarz, A. Buehler, J. Aguirre, V. Ntziachristos, Three-dimensional multispectral optoacoustic mesoscopy reveals melanin and blood oxygenation in human skin in vivo, J. Biophotonics 9 (2016) 55–60, https://doi.org/10.1002/jbio.201500247.
[35] M. Omar, D. Soliman, J. Gateau, V. Ntziachristos, Ultrawideband reflection-mode optoacoustic mesoscopy, Opt. Lett. 39 (2014) 3911–3914, https://doi.org/10.1364/OL.39.003911.
[36] S. Moustakidis, M. Omar, J. Aguirre, P. Mohajerani, V. Ntziachristos, Fully automated identification of skin morphology in raster-scan optoacoustic mesoscopy using artificial intelligence, Med. Phys. 46 (2019) 4046–4056, https://doi.org/10.1002/mp.13725.
[37] M. Stücker, C. Moll, P. Altmeyer, Sauerstoffversorgung der haut, Hautarzt 55 (2004) 273–279, https://doi.org/10.1007/s00105-003-0662-7.
[38] W.C. Vogt, X. Zhou, R. Andriani, K.A. Wear, T.J. Pfefer, B.S. Garra, Photoacoustic oximetry imaging performance evaluation using dynamic blood flow phantoms with tunable oxygen saturation, Biomed. Opt. Express 10 (2019) 449–464, https://doi.org/10.1364/BOE.10.000449.
[39] R. Huggenberger, M. Detmar, The cutaneous vascular system in chronic skin inflammation, J. Investig. Dermatol. Symp. Proc. (2011) 24–32. Elsevier.

Amalina Ebrahim Attia earned her BEng (Hons) in Chemical Engineering from National University of Singapore (NUS). She received her PhD in Drug Delivery from NUS Graduate School for Integrative Sciences and Engineering. She is currently a Research Scientist in Institute of Bioengineering and Bioimaging (IBB), A*STAR, Singapore. Her current research focuses on design and development of pre-clinical and clinical applications for photoacoustic and other optical imaging modalities.

Mohesh Moothanchery graduated with an Integrated Masters in Photonics from Cochin University of Science and Technology (CUSAT), India in 2009. He was awarded his doctoral degree (PhD) from Technological University Dublin (TUD), Ireland in October 2013. He pursued postdoctoral careers at HiLASE Centre, Academy of Sciences of the Czech Republic (ASCR) and Nanyang Technological University (NTU), Singapore before joining Singapore Bioimaging Consortium (SBIC), A*STAR, Singapore in 2017. He is currently a Senior Research Fellow at Institute of Bioengineering and Bioimaging (IBB), A*STAR. His research interests are in the field of optical instrumentation and biophotonics.

Xiuting Li is currently a Research Fellow at Institute of Bioengineering and Bioimaging (IBB), A*STAR. She received her Ph.D. degree in Physics and Applied Physics from School of Physical and Mathematical Sciences (SPMS), Nanyang Technological University (NTU), 2013. Her research interests are bioinformatics, image processing and analysis, machine learning and artificial intelligence.

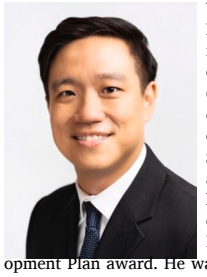

Yik Weng Yew (Asst Prof) is a Consultant Dermatologist at the National Skin Centre (NSC) with strong clinical and research interests in atopic dermatitis (AD), psoriasis dermato-epidemiology and disease outcomes research, with close to 60 peer reviewed scientific publications. He is currently the deputy head of the NSC Research Division and head of Eczema clinic, NSC. He obtained his MBBS from the Yong Loo Lin School of Medicine, NUS in 2006 and completed his training as a dermatologist in 2014 at NSC. After his dermatology training, he obtained a Master of Public Health to further his training in epidemiology research from the Harvard School of Public Health, USA in 2015 as part of his Health Manpower Development Plan award. He was awarded the National Healthcare Group Clinician Scientist Career Scheme award in 2016 and started his PhD studies at Lee Kong Chian School of Medicine, NTU, Singapore to study disease prevalence and risk factors associations of atopic dermatitis in a general adult population cohort. He has also obtained numerous grants, notably the National Medical Research Council (NMRC) New Investigator Grant in 2018 to study treatment of nail psoriasis with microneedles and recently the NMRC Transitional Award in July 2020 to investigate the effects of adiposity on skin barrier function in a general population cohort. He is active in various types of research in AD and collaborates with various local and overseas institutes on population-based cohort studies, clinical trials, basic and translational AD research on omics, skin microbiome and skin bioimaging.

Steven Tien Guan Thng (Assoc Prof) graduated from National University of Singapore in 1992 and went on to pursue his interest in Humanitarian and Disaster medicine with the Singapore Armed Forces from 1992 to 2002. After completing his dermatology training in Singapore, Dr Steven Thng went on to Amsterdam Medical Centre, Netherlands, to continue his training in pigmentary disorder, under Professor Westerhof. Upon returning from his training, Dr Steven Thng started the pigment clinic in National Skin Centre as well as set up the melanocyte culture lab to start his work on cultured melanocytes grafting for vitiligo patients. Currently, Dr Thng is the head of the pigment clinic, in charge of managing all complex pigmentary disorders in National Skin Centre, and he is also the principal surgeon for tissue grafting for vitiligo. In 2012, he has also started a research clinic for hyperpigmentary disorders exploring novel ways to manage difficult hyperpigmentary conditions. He took over as Executive Director of Skin Research Institute of Singapore from Jan 2017 to Feb 2020, and was responsible for the transformation of SRIS from a virtual institute to a dynamic institute, working on 4 main multi-institutional, interdisciplinary research programs of chronic wound, acne, skin microbiome and atopic dermatitis. His current research interest is on skin pigmentary disorder, novel drug delivery systems, as well as advanced imaging for skin cancer and skin diseases. He has translated much of his research to improve patient care in dermatology. He has been serving as the Chief Dermatologist of Skin Research Institute of Singapore from Feb 2020. For his dedication in research and patient care, he was awarded Excellence in Public Service Award in 2013, Healthcare Humanity Award in 2014, Singapore Clinician Investigator Award in 2015 and 2016

U. S. Dinish is the Group Leader in Translational Biophotonics Lab at Institute of Bioengineering and Bioimaging (IBB), A*STAR, Singapore. He also holds a joint visiting faculty position at School of Physical and Mathematical Sciences (SPMS), Nanyang Technological University (NTU), Singapore. He has extensive expertise in various preclinical and clinical studies using photoacoustic imaging, diffuse reflectance spectroscopy (DRS), Raman spectroscopy, surface enhanced Raman scattering (SERS, fluorescence imaging and multimodal imaging approaches. He is the lead PI/Co-PI of many national and international research grants on preclinical and clinical bioimaging/sensing studies. He holds 15 patents/patent applications and has published over 130 international journal papers and conference proceedings. He co-edited a book titled 'frontiers in biophotonics for translational medicine' (Springer) in 2015. Currently, he is serving as the editorial board member of 'Scientific Reports' (Nature Publishing Group) and also as a consulting editor for 'International Journal of Nanomedicine' (Dove press). He is also acting as series editor for Springer's book series titled, 'Progress in Optical Science and Photonics'.

Malini Olivo (Prof) is the Deputy Executive Director and the Director of Biophotonics and Head of the Translational Biophotonics Lab at the Institute of Bioengineering and Bioimaging, A*STAR where she leads efforts to establish a clinical biophotonics translational platform programme. Concurrently, she is also the Executive Director of the A*STAR Health & MedTech Horizontal Technology Programme Office, where she spearheads and coordinates MedTech R&D between A*STAR and the national healthcare ecosystem. Prof. Malini Olivo is also an Adjunct Professor, Lee Kong Chian School of Medicine, NTU and Royal College of Surgeons Ireland, Dublin Ireland. She has published over 400 papers (including several contributions in high impact journals), 3 books and 10 book chapters, and filed 30 patents on technology platforms and devices. She has initiated 3 first-in-human studies using photoacoustic technology in humans for skin and breast cancer and eczema in the last 3 years. She is also founder of 2 MedTech start-ups in Singapore. For her pioneering work on developing biophotonics and decades of experience in translating biophotonics from bench to the clinic, Prof. Malini Olivo was elected to the American Institute for Medical and Biological Engineering (AIMBE) College of Fellows in Washing D.C., U.S.A., in 2019. She is also a fellow member of the Optical Society of America for pioneering and contributing to the field of photomedicine in the seminal area of cancer diagnostics and therapeutics. She is a Fellow of Institute of Physics in UK and Ireland. She champions women in STEM research as a pioneer in the field of biomedical physics.